Supporting Information

Hollowing Integration Engineering to Construct MOF-Derived Carbon Composites for Lightweight and Efficient Microwave Absorption

Zhe Zhang,[a] Jiewu Cui,[*ab] Dongbo Yu,[a] Pengjie Zhang,[c] Wei Sun,[c] Yong Zhang,[a] Song Ma,[d] Xiaohui Liang,[e] Yucheng Wu[*a]

[a] School of Materials Science and Engineering, Key Laboratory of Advanced Functional Materials and Devices of Anhui Province, Hefei University of Technology, Hefei 230009, China

[b] Instrumental Analysis Center, Hefei University of Technology, Hefei 230009, China

[c] BGRIMM Technology Group Co, Ltd, Beijing 102600, China

[d] Shenyang National Laboratory for Materials Science, Institute of Metal Research, Chinese Academy of Sciences, Shenyang 110016, China

[e] Hangzhou Dianzi University, Hangzhou 310018, China

Corresponding author: Jiewu Cui (jwcui@hfut.edu.cn), Yucheng Wu (ycwu@hfut.edu.cn)

Experimental Section

Materials

Cobalt(II) acetate tetrahydrate ($(CH_3COO)_2Co\cdot 4H_2O$), 1,3,5-Benzenetricarboxylic acid ($C_6H_3(CO_2H)_3$, H_3BTC), 2-methylimidazole ($C_4H_6N_2$, Hmim), ethanol were purchased from Sinopharm Chemical Reagent Co., Ltd. Tannic acid ($C_{76}H_{52}O_{46}$, TA) was obtained from Sigma–Aldrich. Deionized water was produced in our laboratory.

Synthesis of Co–BTC nanowires

535.5 mg of $(CH_3COO)_2Co\cdot 4H_2O$ was dissolved in 10 mL of deionized water and 420.3 mg of H_3BTC was dissolved in 90 mL of deionized water, and then the two precursor solutions were mixed and heated to 100 ℃ with magnetic stirring for 15 min. The pink precipitate was then collected by centrifugation, washed three times with ethanol and dried in an oven at 60 °C overnight.

Synthesis of Co–ZIF–SPT

200 mg of Co–BTC nanowire powder obtained above was dispersed in 10 ml of a mixture of deionized water and ethanol ($V_{deionized\ water}$: $V_{ethanol}$ = 9:1) as Solution A. 3 g of 2-methylimidazole (Hmim) was dissolved in a mixture of 30 ml of deionized water and ethanol ($V_{deionized\ water}$: $V_{ethanol}$ = 9:1) as Solution B. After Hmim was completely dissolved, solution B was heated to 75°C. Add solution A to solution B and stir vigorously for 30 min. The purple precipitate was collected by centrifugation, washed three times with ethanol and dried in an oven at 60 °C overnight.

Synthesis of Co–ZIF–HPT and Co–ZIF–HPT–600/700/800

60 mg of Co–ZIF–SPT powder obtained above was homogeneously dispersed in 10 ml of ethanol as Solution A. 300 mg of tannic acid was dissolved in 40 ml of a mixture of deionized water and ethanol ($V_{deionized\ water}$: $V_{ethanol}$ = 1:1) as Solution B. Solution A was added to solution B and the reaction was carried out under magnetic stirring for 20 min at room temperature. The precipitate was collected by centrifugation, washed three times with ethanol and dried in an oven at 60 °C overnight.

Synthesis of Co–ZIF–SPT–700 and Co–ZIF–HPT–600/700/800

The obtained Co–ZIF–SPT powder was placed in a tube furnace and heated to 700

℃ (2 ℃/min) in an argon atmosphere and held for 2 h, and then cooling to room temperature. The as–prepared samples were labeled Co–ZIF–SPT–700. The obtained Co–ZIF–HPT–C powder was placed in a tube furnace and heated to 600/700/800 ℃ (2 ℃/min) in an argon atmosphere and held for 2 h, and then cooling to room temperature. The as–prepared samples were labeled Co–ZIF–HPT–600/700/800.

Characterization

The morphology, microstructure and elemental distribution of the samples were characterized by Field-emission scanning electron microscopy (FESEM, Regulua 8230), Transmission electron microscopy (TEM, JEM–1400flash) and high-resolution transmission electron microscopy (HETEM, Talos F200X G2) with energy dispersive X-rays spectroscopy (EDX). The crystal structure and phase composition of the samples were investigated using an X-ray diffractometry (XRD, Rigaku D/MAX2500VL/PC). The Raman spectrum of the samples were measured by a micro confocal laser Raman spectrometer (LabRAM HR Evolution) with a laser wavelength of 532 nm. X-ray photoelectron spectroscopy (XPS, ESCALAB 250Xi) with the aid of a monochromatic Al K_{α} X-ray source was used to characterize the chemical components and elemental valence states of the sample surface. Hysteresis lines were measured at room temperature with a vibrating sample magnetometer (VSM, LakeShore7407). The specific surface area and pore size distribution of the samples were analyzed at 77 K using a gas adsorption analyzer (Autosorb–IQ3).

To measure the electromagnetic properties, the samples powder (Co–ZIF–SPT–700, Co–ZIF–HPT–600/700/800) (10 wt%) was homogeneously mixed with molten paraffin wax (90 wt%), which were pressed to form ring samples (7.00 mm outer diameter, 3.04 mm inner diameter and 2.0 mm thickness). Based on the coaxial line theory, the electromagnetic parameters of the prepared samples were measured in the frequency range of 2–18 GHz using a vector network analyzer (ROHDE&SCHWARZ, ZNA43).

Equations

The reflection loss (RL) values can be calculated according on the transmission line theory by equation S1 and equation S2

$$Z_{in} = Z_0\sqrt{\mu_r/\varepsilon_r}\tan h\left[j(2\pi f d/c)\sqrt{\mu_r\varepsilon_r}\right] \quad \text{(S1)}$$

$$RL(dB) = 20\log\left|(Z_{in} - Z_0)/(Z_{in} + Z_0)\right| \quad \text{(S2)}$$

where, Z_0, Z_{in}, c, d, and f represent the impedance of free space, the input characteristic impedance of the composite, the velocity of light in vacuum, the thickness of the hybrid composite and the frequency of the microwave, respectively. ε_r and μ_r represent the complex permittivity and complex permeability.

According to the Debye theory, the Cole–Cole curve (ε″ vs. ε′) shows the polarization relaxation process in the absorber. Complete semicircles in the curve suggest Debye relaxation processes in the material.

$$(\varepsilon' - \frac{\varepsilon_s + \varepsilon_\infty}{2})^2 + (\varepsilon'')^2 = \left(\frac{\varepsilon_s - \varepsilon_\infty}{2}\right)^2 \quad \text{(S3)}$$

where, ε_S and ε_∞ stand the static permittivity and the relative permittivity at infinite frequency.

According to equation S4, if the magnetic loss is solely caused by eddy current loss, then the calculated eddy current coefficient (C_0) should stay constant even when the frequency increases.

$$C_0 = \mu''(\mu')^{-2}f^{-1} \quad \text{(S4)}$$

The equation for calculating Z can be expressed as follows.

$$Z = \left|\frac{Z_{in}}{Z_0}\right| = \sqrt{\mu_r/\varepsilon_r}\tan h\left[j(2\pi f d/c)\sqrt{\mu_r\varepsilon_r}\right] \quad \text{(S5)}$$

Quarter-wavelength modeling equation.

$$t_m = \frac{n\lambda}{4} = \frac{nc}{4f_m\sqrt{|\mu_r||\varepsilon_r|}}\,(n = 1, 3, 5, 7\cdots) \quad \text{(S6)}$$

where λ, t_m and f_m represent the wavelength, the matching thickness, and the matching frequency.

The attenuation constant (α) is capable of comprehensively evaluating the absorber's ability to attenuate electromagnetic waves.

$$\alpha = \frac{\sqrt{2}\pi f}{c}\sqrt{(\mu''\varepsilon'' - \mu'\varepsilon') + \sqrt{(\mu''\varepsilon'' - \mu'\varepsilon')^2 + (\mu'\varepsilon'' + \mu''\varepsilon')^2}} \quad \text{(S7)}$$

Radar Cross Section (RCS) Simulation

The RCS of Co–ZIF–HPT–600/700/800 are simulated using CST Studio Suite 2019 software to verify the respective attenuation properties. The simulation models consisted of a double-layer composite plate consisting of a perfect electric conductor layer (PEC) (200 × 200 mm) and an absorber coating layer (200 × 200 mm). The simulated frequency is set to 8.96 GHz, the thickness of the coated absorber are set to 3.14 mm, and the thickness of the PEC plates are all set to 1 mm, respectively. The simulated models are placed in the XOY plane to receive incident electromagnetic waves from the negative direction of the Z-axis. The scattering direction is determined by θ and φ using open boundary conditions in this direction. The RCS values can be calculated by the following equation:

$$\sigma\left(dB\ m^2\right) = 10\log\left(\frac{4\pi S}{\lambda^2}\left|\frac{E_s}{E_i}\right|^2\right) = 10\log\left(\frac{4\pi S}{\lambda^2}\left|\frac{H_s}{H_i}\right|^2\right) \quad \text{(S8)}$$

where S and λ are the area of the simulation model and the wavelength of the electromagnetic wave, E_s and E_i are the scattered and incident electric field strengths, and H_s and H_i are the scattered and incident magnetic field strengths.

Power Loss Density Simulation

The power loss density of Co–ZIF–HPT–600/700/800 are simulated using CST Studio Suite 2019 software. The simulation models are constructed as square plates (10 × 10 × 3.14 mm) in the X–O–Y plane at the detection frequency of 8.96 GHz. Periodic boundary conditions are imposed in the X and Y directions, with an open boundary (plus space) in the positive Z-axis direction and a potential boundary condition (electric E_t=0) in the negative Z-axis direction.

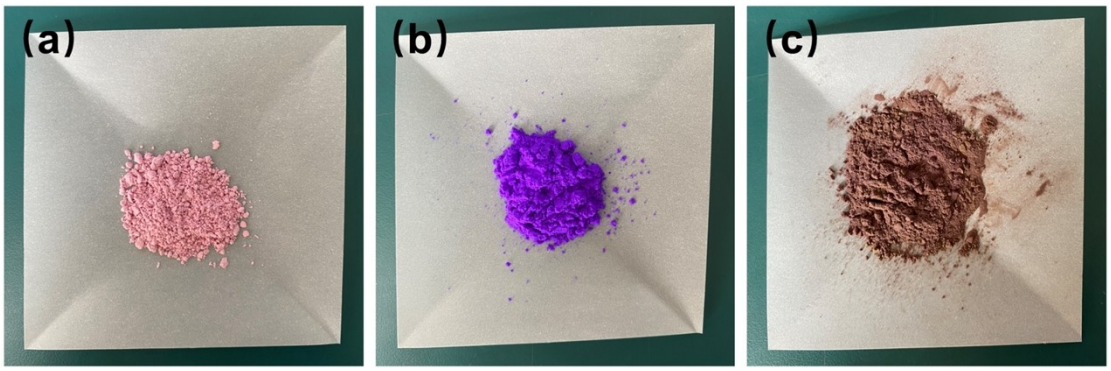

Figure S1. a) Co-BTC sample. b) Co-ZIF-SPT sample. c) Co-ZIF-HPT sample.

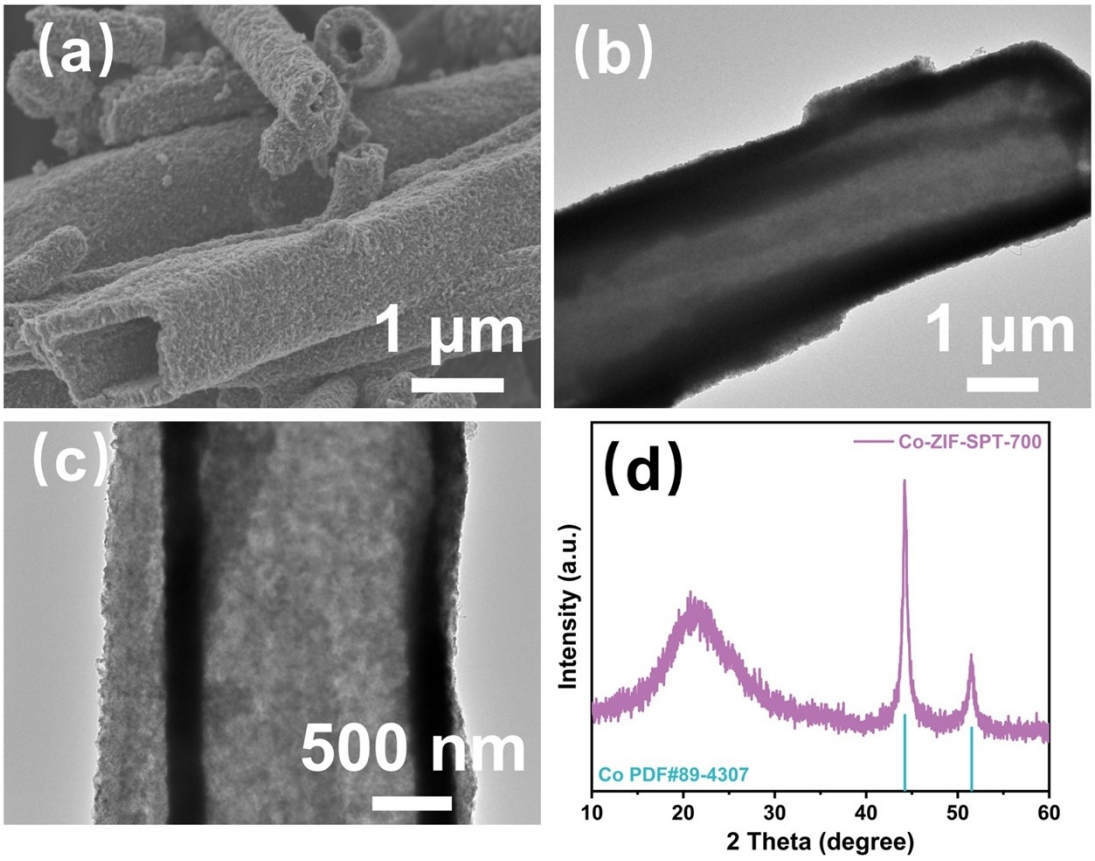

Figure S2. a) SEM image, b–c) TEM images and d) XRD pattern of Co–ZIF–SPT–700.

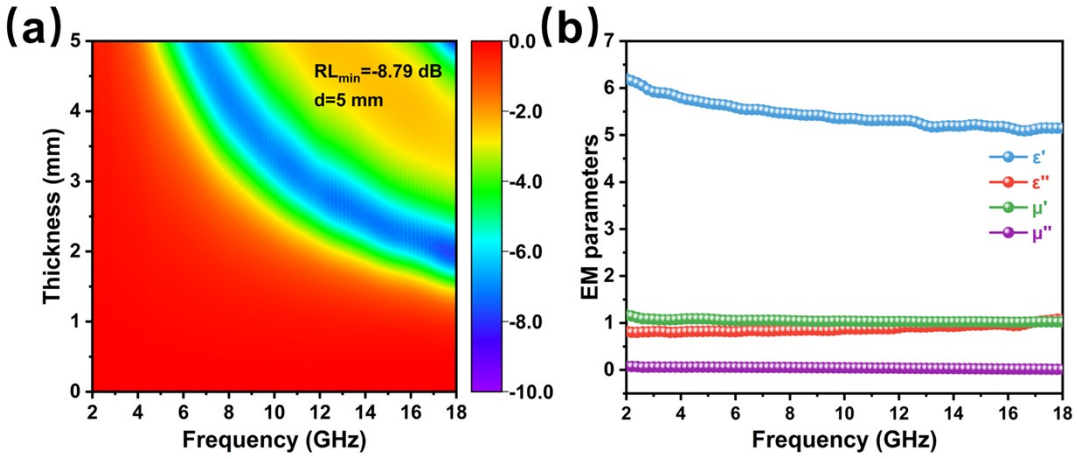

Figure S3. a) 2D RL contour map, b) electromagnetic parameters of Co–ZIF–SPT–700.

Table S1. Comparison of electromagnetic wave absorption performance of this work with other similar absorbers

Samples	RL_{min} (dB)/ thickness (mm)	EAB (GHz)/ thickness (mm)	$\|RL_{min}\|\cdot$EAB/filling ration	Refs
ZnO/Carbon porous nanofibers	–22.89/1.5	5.64/2.5	645.50	[1]
Co/C–700	–30.12/3	4.93/3	593.97	[2]
1.2Ni–HMCNTs–700	–50.4/3.1	7.32/2.95	3689.28	[3]
H–Co_7Fe_3/Co@NC	–59.70/3	6.01/2.1	896.99	[4]
Fe_3O_4@PBA	–57.01/3.6	4.58/4	1305.53	[5]
Fe–SAs/NC	–52.5/2.8	4.8/1.7	1008	[6]
Fe_2N@CNTs	–54.55/3.43	5.52/1.82	752.79	[7]
Ni@B/N–0.195	–56.9/5.69	7.12/5.69	4051.28	[8]
HPCN–3	–18.13/1.6	5.17/1.6	374.93	[9]
Fiber–Rob	–57.1/4.6	2.3/2.9	525.32	[10]
BCN/C/Co–1.5	–56.7/2.9	5.5/2.6	649.69	[11]
Co/C@Ag NMs	–44.5/3	1.28/3.5	189.87	[12]
Co–ZIF–HPT–700	**–76.93/3.14**	**6.28/2.12**	**4831.20**	**This work**

Notes and references

1. W. Gu, J. Lv, B. Quan, X. Liang, B. Zhang and G. Ji, *J. Alloys Compd.*, 2019, **806**, 983-991.
2. H. Wang, L. Xiang, W. Wei, J. An, J. He, C. Gong and Y. Hou, *ACS Appl. Mater. Interfaces*, 2017, **9**, 42102-42110.
3. L. Chen, J. Pan, T. Wang, W. Xia, J. He and K. Zhang, *Adv. Funct. Mater.*, 2024, 2409432.
4. X. Zhou, X. Wu, S. Li, Y. He, R. Wang, S. Rao, Q. Zhuang, Y. Zhou, X. Liu and P. Zuo, *Carbon*, 2024, **230**,119592.
5. J. Xiao, B. Wen, J. Li, X. Liu, S. Xue, Z. Wei, S. Yang, G. Yang and S. Ding, *J. Alloys Compd.*, 2024, **1008**, 176595.
6. Y. Su, B. Jiang, H. Shen, N. Yang, X. Tantai, X. Xiao, Y. Sun and L. Zhang, *Carbon*, 2025, **231**, 119699.
7. J. Wang, Z. Miao, K. Gao, Z. Li, X. Zhang, C. Yang, S. Iqbal, G. Xiang, A. Cui, L. Liu, C. Sun, H. Wu and J. Y. Yang, *Adv. Funct. Mater.*, 2024, **34**, 2408696.
8. M. Li, Y. Zhang, Z. Chen, Y. Zhang, B. Yang, F. Xie, X. Gong, T. Zhang and X. Huang, *Chem. Eng. J.*, 2024, **483**, 149151.
9. J. Tao, J. Zhou, Z. Yao, Z. Jiao, B. Wei, R. Tan and Z. Li, *Carbon*, 2021, **172**, 542-555.
10. M. Li, X. Song, J. Xue, F. Ye, L. Yin, L. Cheng and X. Fan, *ACS Appl. Mater. Interfaces*, 2023, **15**, 31720-31728.
11. C. Jiang and B. Wen, *Small*, 2023, **19**, 2301760.
12. H. Tian, J. Qiao, Y. Yang, D. Xu, X. Meng, W. Liu, X. Zhang, B. Li, L. Wu, Z. Zeng and J. Liu, *Chem. Eng. J.*, 2022, **450**, 138011.